

# Deterministic and Probabilistic Predictions of Yield Strength and Inelastic Displacement Spectra

Yousef Bozorgnia,<sup>a)</sup> M.EERI, Mahmoud M. Hachem,<sup>b)</sup> M.EERI,  
and Kenneth W. Campbell,<sup>c)</sup> M.EERI

This paper presents deterministic and probabilistic predictions of inelastic response spectra based on a comprehensive ground motion prediction equation (GMPE). Our analysis reveals that over a wide structural period range, the magnitude scaling for an inelastic system is higher than that for an elastic system, especially for ductility levels greater than 2 and magnitude greater than 6.5. Both deterministic and probabilistic hazard analyses show that the “equal displacement rule,” to estimate inelastic displacement, is valid for small to moderate magnitudes and/or for low ductility levels. However, it underestimates inelastic deformation even for long period structures if the earthquake magnitude is large and the structure needs to sustain a large ductility. Our study shows that an inelastic GMPE can easily be implemented as part of standard probabilistic seismic hazard analysis (PSHA) packages to directly generate probabilistic hazard for inelastic response, avoiding possible over- or under-conservatism in approximating inelastic deformation from an elastic system. [DOI: 10.1193/1.3281659]

## INTRODUCTION

In the companion paper that appears in this issue (Bozorgnia et al. 2010), we presented the methodology and validation of the development of a comprehensive ground motion prediction equation (GMPE), or “attenuation” relationship, for inelastic response spectra. We developed a large database of inelastic response spectra using a subset of the PEER NGA strong motion database. Our selected database includes 3122 horizontal records from 64 earthquakes with moment magnitudes ranging from 4.3–7.9 and rupture distances ranging from 0.1–199 km. Using this comprehensive database of “constant ductility” spectra, we developed GMPEs for different levels of displacement ductility ranging from one (i.e., elastic response) to eight. For each ductility level, the GMPE correlates inelastic spectra to earthquake magnitude, fault mechanism, fault distance, local soil conditions, and basin (sediment) depth.

In this paper, we use the developed GMPEs to predict yield strength and inelastic displacement spectra as a function of source, path and site parameters. We further use

---

<sup>a)</sup> Executive Director, Pacific Earthquake Engineering Research Center (PEER), 325 Davis Hall, University of California, Berkeley, CA 94720-1792. yousef@berkeley.edu

<sup>b)</sup> Senior Structural Engineer, Skidmore, Owings and Merrill LLP, San Francisco, CA 94111

<sup>c)</sup> Senior Vice President, EQECAT, Inc., Beaverton, OR 97006

the GMPE in a probabilistic seismic hazard analysis (PSHA) computer code to directly carry out PSHA on inelastic response spectra. Example PSHA results are presented in this paper for a site in San Francisco, California.

By analyzing a comprehensive database of inelastic spectra, we examine the relationship between the predicted inelastic and elastic displacement spectra, and the sensitivity of such a relationship to various fundamental parameters such as earthquake magnitude and fault rupture distance. We also examine the range of the validity of the traditional assumptions, such as the classic “constant displacement rule,” that has been extensively used in earthquake engineering.

Details of the model development can be found in [Bozorgnia et al. \(2010\)](#); however, for the sake of self-sufficiency, we recall a few basic definitions (see, e.g., [Bozorgnia and Campbell 2004](#)). The subject structural model is a single-degree-of-freedom (SDF) inelastic system with an elastic-perfectly-plastic force-deformation relationship. The key parameters of the inelastic system are defined as follows: yield strength  $F_y$ ; yield deformation  $u_y$ ; and maximum deformation  $u_{max}$  (relative to the ground). The system ductility is defined as  $\mu = u_{max}/u_y$ . We used a 5% viscous damping ratio.

In this paper, we first present the median prediction results for normalized yield strength  $F_y/W$  spectra, where  $W$  is the weight of the system. This is followed by a presentation of the predicted maximum inelastic displacement  $u_{max}$  as a function of fundamental parameters defining source, path and site effects. We then examine the relationship between elastic and inelastic displacements. Finally, we present examples of PSHA results for the yield strength and inelastic displacement of the model structure for a site in San Francisco.

## PREDICTION OF YIELD STRENGTH SPECTRA

Selected results of the median prediction of the yield strength spectra are presented in this section. Figure 1 shows complete median inelastic spectra for the normalized yield strength  $F_y/W$  at a site with  $V_{s30} = 760$  m/s located at rupture distances 1 and 10 km from a strike-slip fault of magnitude 7.5 for  $\mu = 1, 2, 4, 6$  and 8. For comparison purposes, median elastic spectra predicted by the [Campbell and Bozorgnia \(2008\)](#) GMPE developed as part of the Next Generation Attenuation (NGA) project, are also plotted with dashed lines. At short and moderate periods the results of the current study for  $\mu = 1$  are very consistent with those predicted by [Campbell and Bozorgnia \(2008\)](#). A more detailed comparison of these two elastic displacement spectra at long periods will be presented in the next section.

Consistent with previous nonlinear analysis studies (e.g., [Newmark and Hall 1982](#), among others), it is evident from Figure 1 that the strength demand can be substantially reduced if a moderate level of ductility (e.g.,  $\mu = 2$ ) is sustained by the structure. Larger available ductility can only result in a moderate reduction in the strength demand.

Effects of style of faulting on inelastic spectra are presented in Figures 2 and 3. These figures are for  $\mu = 4$ . Figure 2 presents the scaling of ground motion with near-source distance revealing the effects of style-of-faulting, hanging wall, and footwall. These figures show that for reverse faulting, if the coseismic fault rupture does not reach

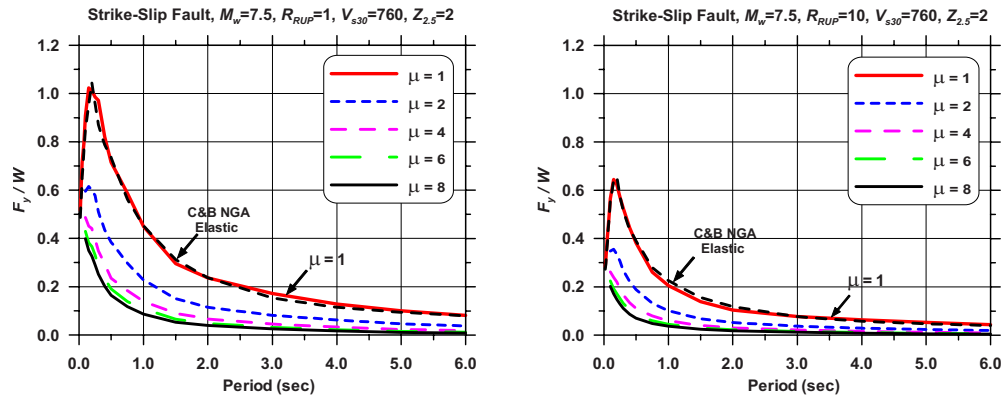


**Figure 1.** Median inelastic spectra for  $F_y/W$  at a site with  $V_{s30}=760$  m/s located at rupture distances  $R_{RUP}=1$  km (left), and 10 km (right) from a strike-slip fault for magnitude 7.5. Each case has spectra for ductility  $\mu=1, 2, 4, 6$  and 8. For comparison, median elastic NGA spectra predicted by [Campbell and Bozorgnia \(2008\)](#) are also plotted.

the ground surface (i.e.,  $Z_{TOR} > 0$ ), the inelastic demand is higher than for the case with surface rupture. Unsymmetrical curves in Figure 2 (with respect to the vertical axis) are indicative that hanging wall sites are subjected to higher inelastic demands than those at the footwall. Figure 3 shows these effects over a wide period range. In this figure, the effects of style of faulting, i.e., strike-slip, reverse (with and without surface rupture), and normal faulting, as well as hanging wall/footwall effects are presented. Figure 3 shows that earthquakes with different styles of faulting demand different yield strengths on systems with periods shorter than about 1.5 sec when the hanging wall effects are included. The trends presented

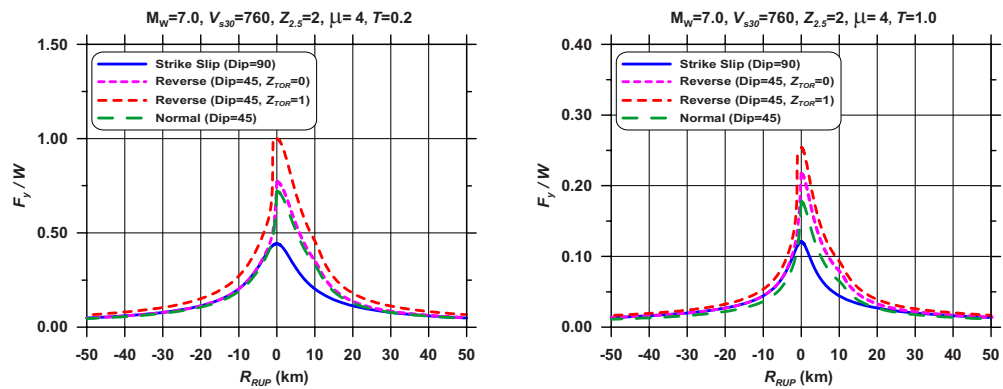


**Figure 2.** Effects of style of faulting and hanging-wall/footwall site locations for  $M=7.0$ . The plots are for ductility  $\mu=4$ , at periods 0.2 sec (left) and 1.0 sec (right). “Positive distances” denote site locations on hanging-wall, and “negative distances” denote site locations on footwall.

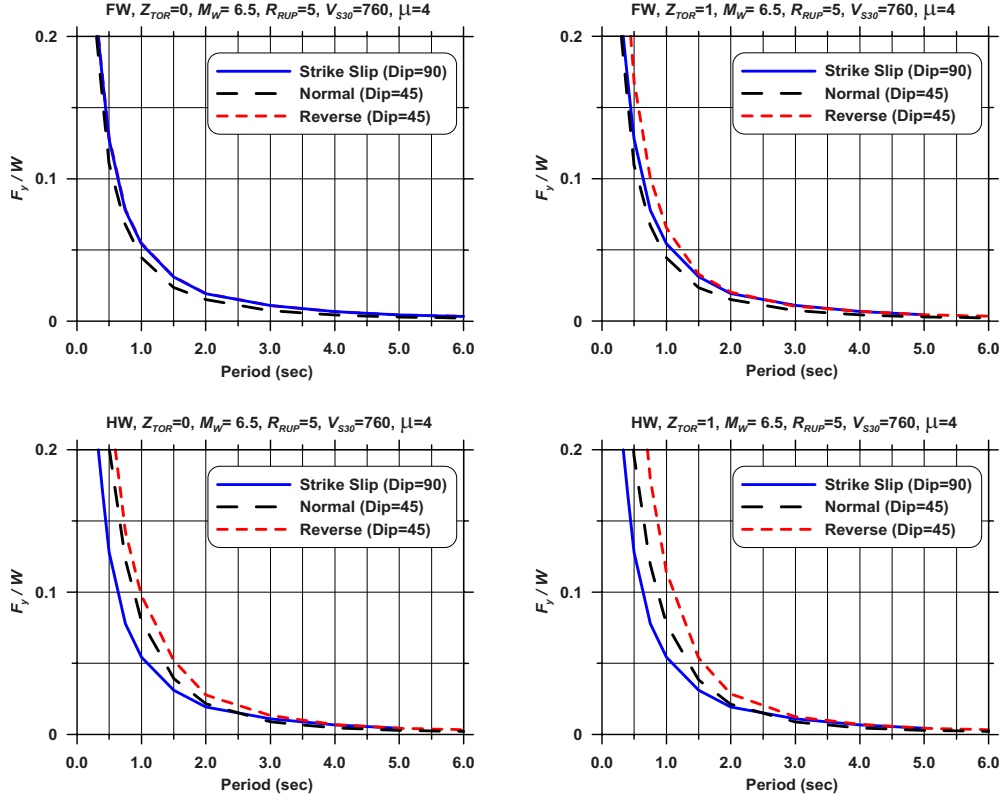


**Figure 3.** Effects of style of faulting and hanging-wall/footwall on inelastic response spectra. The plots are median inelastic spectra for  $F_y/W$  for ductility  $\mu=4$ , at a site with  $V_{S30}=760$  m/s located at rupture distance of 5 km, for a magnitude 6.5 earthquake. Top frames are for footwall (FW) and bottom frames for hanging wall (HW) sites. Left frames are for the case in which the fault rupture reached the surface ( $Z_{TOR}=0$ ), and right frames are for  $Z_{TOR}=1$  km.

in Figures 2 and 3 for inelastic spectra are qualitatively consistent with those for elastic spectra (Campbell and Bozorgnia 2007, 2008). Also similar to the case of the NGA elastic, the results for normal faulting are less constrained than those for strike-slip and reverse faults, as the database includes much smaller number of normal faulting events than strike-slip and reverse events.

Local site effects, in terms of the average shear-wave velocity in top 30-m of soil ( $V_{S30}$ ) are presented in Figure 4. The  $V_{S30}$  values in this figure (150, 255, 525, 1,070 m/sec) are representative of NEHRP site classes E, D, C, and B respectively. As this figure shows, at moderate and long periods, the strength demand on the inelastic system increases with decreasing  $V_{S30}$ . This behavior is qualitatively consistent with the site effects on elastic spectra (Campbell and Bozorgnia 2007, 2008). The variations of the soil amplification factors for various values of  $V_{S30}$  are plotted in Figure 5. In this figure, “site amplification” is defined as the ratio of  $(F_y/W)$  for various  $V_{S30}$  values, over that for  $V_{S30}=1,070$  m/sec. The dashed

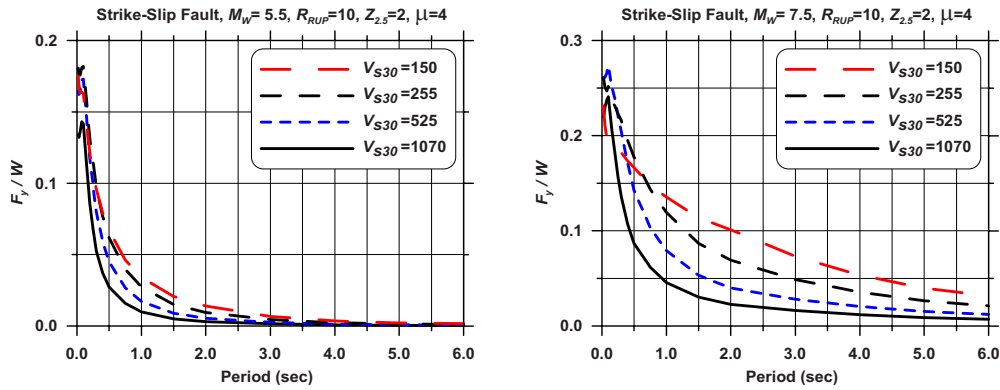


**Figure 4.** Effects of  $V_{s30}$  (site effects) on median inelastic spectra for  $F_y/W$  for ductility  $\mu=4$ , at a site located at distance 10 km from a strike-slip fault for magnitude 5.5 (left) and 7.5 (right).

lines in this figure are for the acceleration response spectra predicted by the NGA relationships of [Campbell and Bozorgnia \(2007, 2008\)](#). Figure 5 shows that the site amplifications for elastic and inelastic response spectra are comparable, with a minor difference at longer periods and lower shear-wave velocities.

Effects of soil nonlinear response on the site amplifications are presented in Figure 6 for  $\mu=4$ . The site amplifications in this figure are for the same NEHRP site categories as in Figures 4 and 5. It is evident that by increasing the severity of the input motion, as

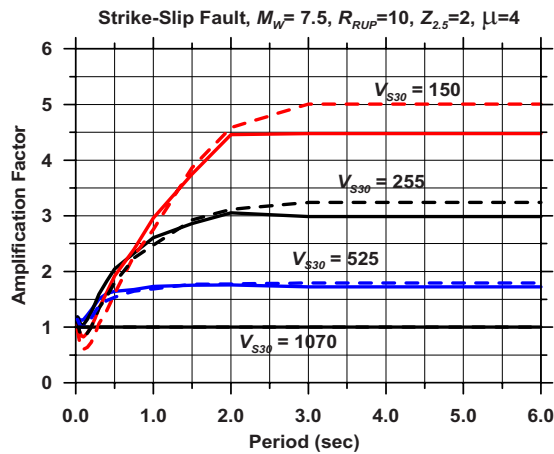


**Figure 5.** Site amplification effects on median inelastic spectra for  $F_y/W$  for ductility  $\mu=4$  (solid lines), at a site located at distance 10 km from a strike-slip fault for magnitude 7.5. Dashed lines are for the corresponding site amplification for elastic NGA by [Campbell and Bozorgnia \(2008\)](#).

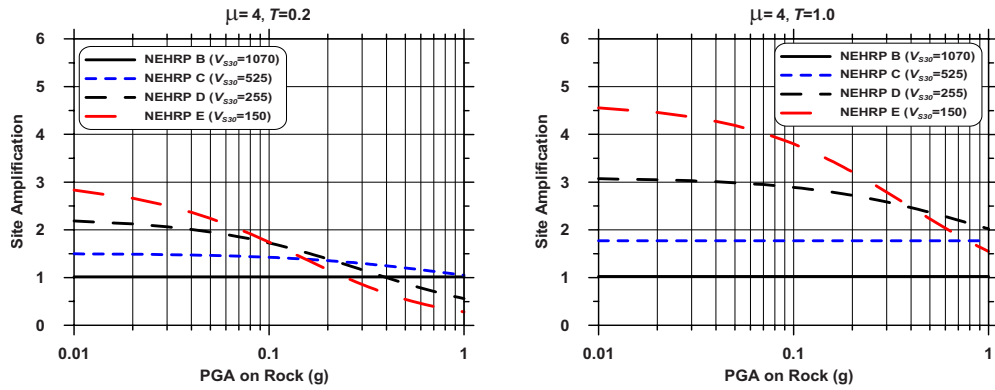


**Figure 6.** Shallow site amplification scaling with rock PGA (i.e.,  $A_{1100}$ ) for ductility  $\mu=4$ , at periods 0.2 sec (left) and 1.0 sec (right).

measured in this figure in terms of PGA on rock, the site amplification reduces, especially for softer soils. The reduction in amplification is due to the soil nonlinear behavior. This concept is qualitatively consistent with that for elastic structural response as reported by [Campbell and Bozorgnia \(2007, 2008\)](#).

Finally, the effects of sediment depth, i.e., basin effects, are shown in Figure 7. This figure shows the normalized yield strength ( $F_y/W$ ) spectra for  $\mu=4$  for sediment depths ( $Z_{2.5}$ ) of 0, 2, and 5 km, for  $V_{s30}=255$  m/sec (representative of the NEHRP site class D).

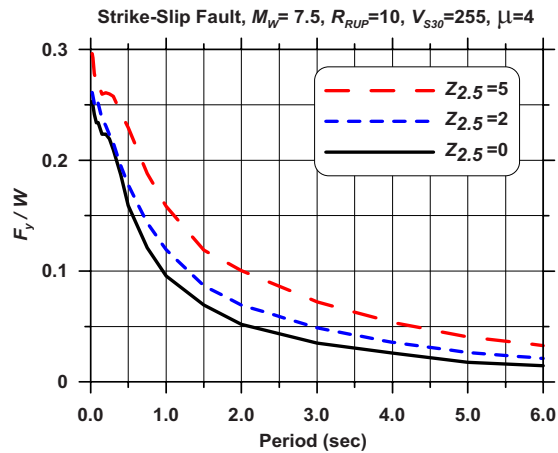


**Figure 7.** Effects of  $Z_{2.5}$  (basin effects) on median inelastic spectra for  $F_y/W$  for ductility  $\mu=4$ , at a site with NEHRP “D” site condition located at distance 10 km from a strike-slip fault for magnitude 7.5.

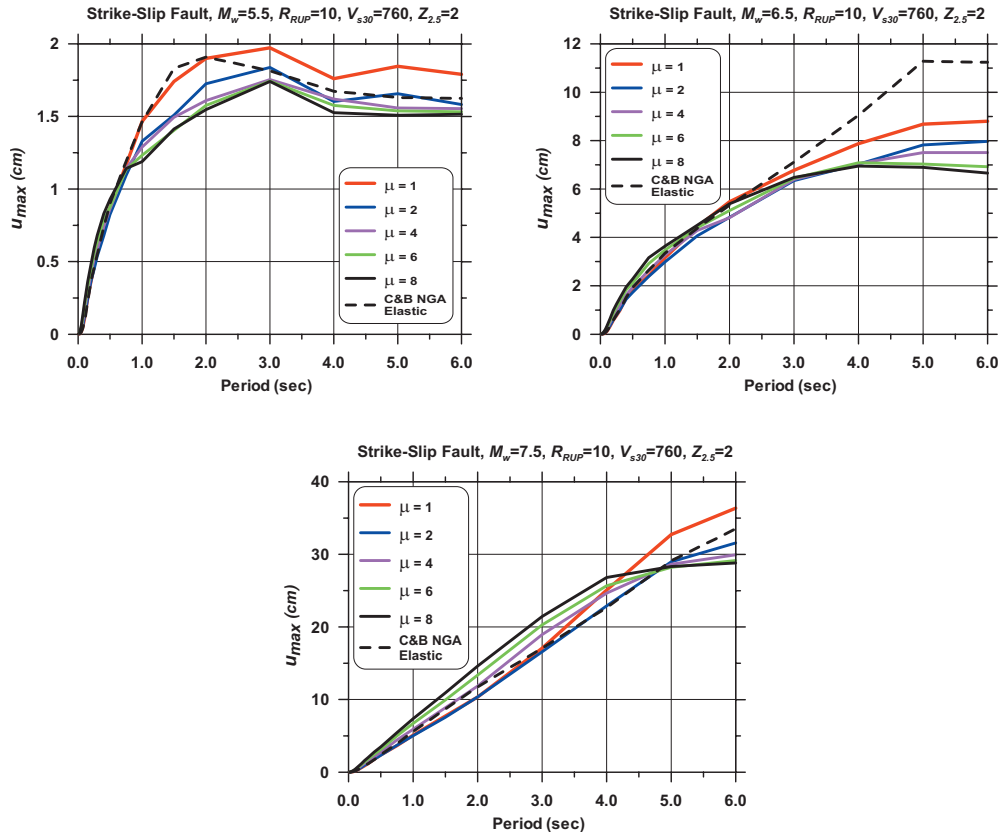


**Figure 8.** Median displacement spectra ( $u_{max}$ ) at a site with  $V_{s30}=760$  m/sec located at rupture distance 10 km from a strike-slip fault of magnitudes 5.5 (top left), 6.5 (top right) and 7.5 (bottom). Each frame has spectra for ductility  $\mu=1, 2, 4, 6$  and 8, and NGA elastic prediction by [Campbell and Bozorgnia \(2008\)](#).

By increasing the sediment depth, the yield strength demand increases. This is also conceptually consistent with the effect of sediment depth on the elastic spectra, especially at longer periods ([Campbell and Bozorgnia 2007, 2008](#)).

### PREDICTION OF INELASTIC DISPLACEMENT SPECTRA

In this section, we present the results of our prediction of inelastic displacement demands. Figure 8 shows median values of the maximum displacements at a site located at 10 km from a strike-slip fault for moment magnitudes 5.5, 6.5, and 7.5. The displacement spectra plotted in this figure are for  $\mu=1, 2, 4, 6,$  and 8. Given the ductility ratio and period of the system, inelastic displacement demand and yield strength are related through the definition of ductility ratio and the fact that  $F_y$  is the product of  $u_y$  and the initial elastic stiffness. For comparison, Figure 8 also shows the elastic displacement spectra predicted by the [Camp-](#)

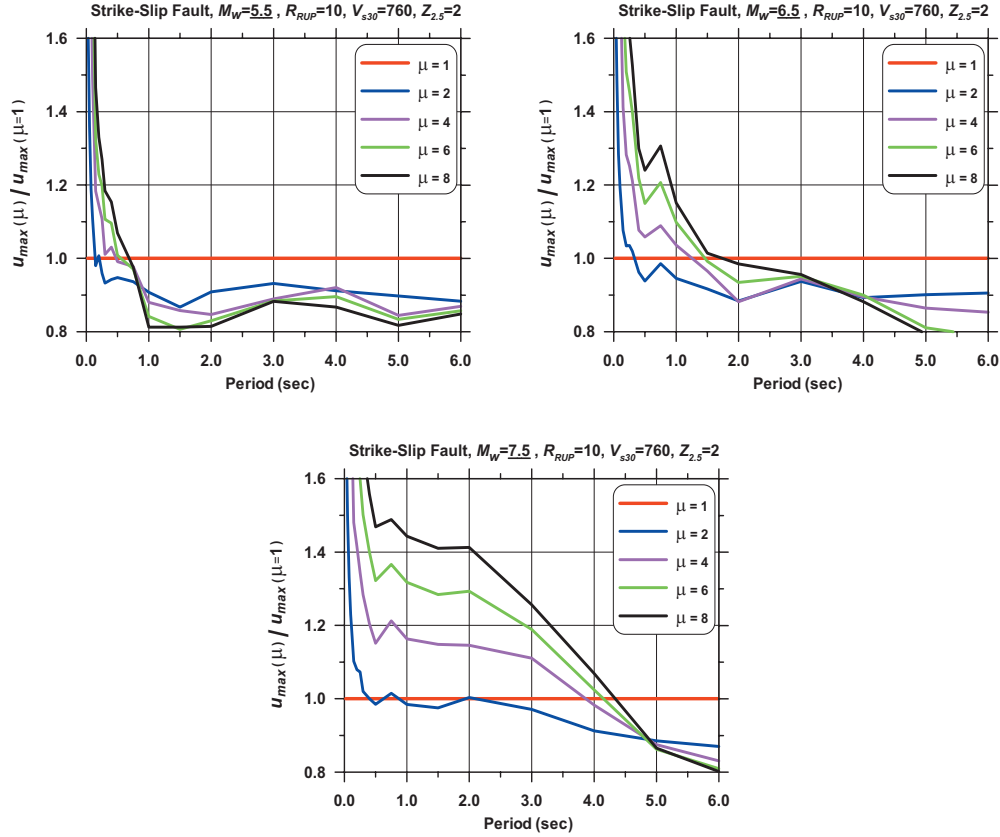


**Figure 9.** Ratio of median displacement for a ductility  $\mu$  over that for  $\mu=1$ , for magnitude 5.5 (top left), 6.5 (top right), and 7.5 (bottom) for  $R_{RUP}=10$  km.

bell and Bozorgnia (2007, 2008) NGA relationships. There is a difference between the displacement predicted for  $\mu=1$  and that by the NGA relationship at low and moderate magnitudes. This is mainly due to the seismological constraints that were applied to the regression coefficients in the NGA elastic GMPE at long periods (see Campbell and Bozorgnia 2007, 2008 for details). In the current study, we applied very limited constraints on the computed coefficients. Figure 8 also shows that the shape of elastic and inelastic displacement spectra is a function of magnitude. By increasing magnitude, the spectral peak shifts to longer periods, as larger magnitude earthquakes tend to be richer in long-period ground motions than smaller events.

To examine the relative differences between the spectra of inelastic and elastic displacements, Figure 9 presents the ratio of the maximum inelastic displacement over the displacement for  $\mu=1$  for various magnitudes and ductility levels. This ratio is also called “inelastic displacement, or deformation, ratio” (e.g., Miranda 2000, Chopra and Chintanapakdee 2004). Figure 9 is for a distance of 10 km from the earthquake source.

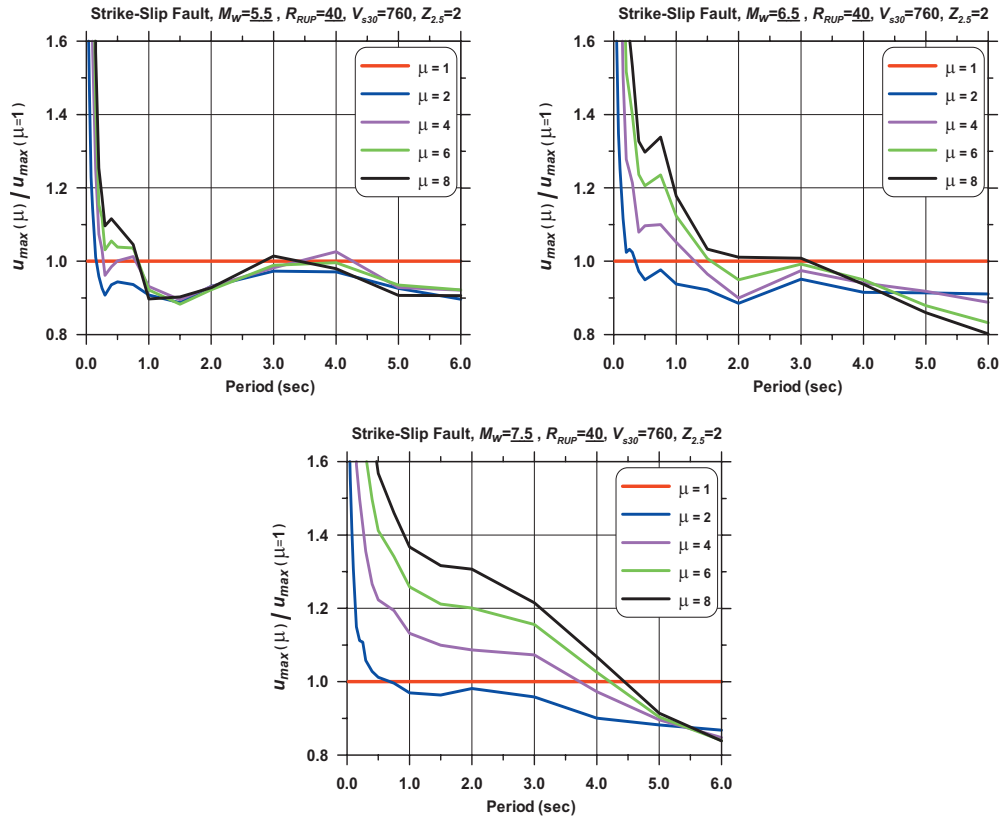


**Figure 10.** Ratio of median displacement for a ductility  $\mu$  over that for  $\mu=1$ , for magnitude 5.5 (top left), 6.5 (top right), and 7.5 (bottom) for  $R_{RUP}=40$  km.

Figure 10 presents similar results for a distance of 40 km. These figures show that for periods longer than some “crossing period” the maximum displacement is less sensitive to ductility, and in fact the maximum displacement decreases with increasing ductility, and as a special case, the elastic displacement is larger than the inelastic displacement.

An important revelation in Figures 9 and 10 is that the crossing period is a function of earthquake magnitude, and it shifts to longer periods by increasing magnitude. The crossing period is around 0.5–1 sec, 3–4.5 sec, and 5–5.5 sec for magnitudes 5.5, 6.5, and 7.5, respectively. For periods shorter than the crossing period, the ratio of inelastic over elastic displacements increases with increasing ductility, and shorter periods correspond to a wider difference between elastic and inelastic displacements. As an example, for an earthquake of magnitude 7.5 and a period of 2.0 sec, the median of maximum inelastic displacement for  $\mu=6$  is about 20–30% larger than that for elastic system.

Figures 9 and 10 also reveal that in the ranges of parameters of most concern, the ratio of inelastic to elastic displacements is more sensitive to magnitude than distance.

This is qualitatively consistent with the results presented by [Tothong and Cornell \(2006\)](#); however, at long periods our results show stronger magnitude dependency than their study. Other previous studies either concluded that median inelastic displacement ratio is relatively independent of both magnitude and distance (e.g., [Chopra and Chintanapakdee 2004](#), [Miranda 2000](#)), or did not investigate the magnitude scaling (e.g., [FEMA 440 2005](#)). Analysis of a very large database of inelastic spectra has enabled us to trace the sensitivity of the inelastic displacement ratio to various parameters such as earthquake magnitude, site-to-source distance, among other parameters.

We are now in the position to re-examine the pioneering concept of the “equal displacement rule” proposed decades ago by Veletsos, Newmark, and Hall ([Veletsos and Newmark 1960](#), [Riddell 2008](#)). [Newmark and Hall \(1982\)](#) summarized the concept as follows: “*For low frequencies, corresponding to about 0.3 Hz as an upper limit [periods longer than 3.3 sec], displacements are preserved. In fact, the inelastic system may have perhaps even a smaller total displacement than elastic systems. For frequencies between about 0.3 to about 2 Hz [periods between about 0.5 and 3.3 sec] the displacements are very nearly the same for all ductility factors*” (words in brackets are ours). This is the classic “equal displacement rule” which has been used as the basis of seismic design of many structural systems worldwide.

As Figures 9 and 10 show, we can definitely confirm the equal displacement rule; however, its period range of validity is a function of earthquake magnitude and ductility level. We should be especially careful in using the equal displacement rule if the earthquake magnitude is large and the structure needs to sustain a large ductility. For example, as shown in Figures 9 and 10, for a magnitude of 7.5 and  $\mu=6$ , the equal displacement rule can result in an unconservative estimate of the inelastic displacement over a wide period range shorter than about 3.0 sec. On the other hand, for the same earthquake, we can comfortably use the equal displacement rule for  $\mu=2$  and periods longer than about 0.5 sec.

As mentioned above, for a given ductility level, and at periods shorter than a “crossing period,” the ratio of inelastic over elastic displacement increases with increasing the magnitude. In other words, by increasing magnitude, although both elastic and inelastic displacements increase, the inelastic displacement increases more than the elastic displacement. This means that the scaling of inelastic displacement with magnitude is larger for an inelastic system than for the elastic system. We explicitly examine this issue in Figure 11, which shows the trends in increasing the maximum displacement due to increasing magnitude by one unit. Figure 11 reveals that over a wide period range, *magnitude scaling is higher at higher ductility levels*, and as a special case, magnitude scaling for inelastic systems (especially for  $\mu > 2$ ) is higher than that for elastic systems. Consequently, it is generally unconservative to use the magnitude scaling model for an elastic system and apply it to an inelastic system, as is a common practice in performing seismic hazard analyses for elastic response spectra and using these results to predict inelastic response spectra. The degree of such an unconservatism depends on the level of ductility, as elaborated below. Also, by comparing the top right and top left frames in Figure 11, we observe that in the ranges of the parameters of most interest, the magni-

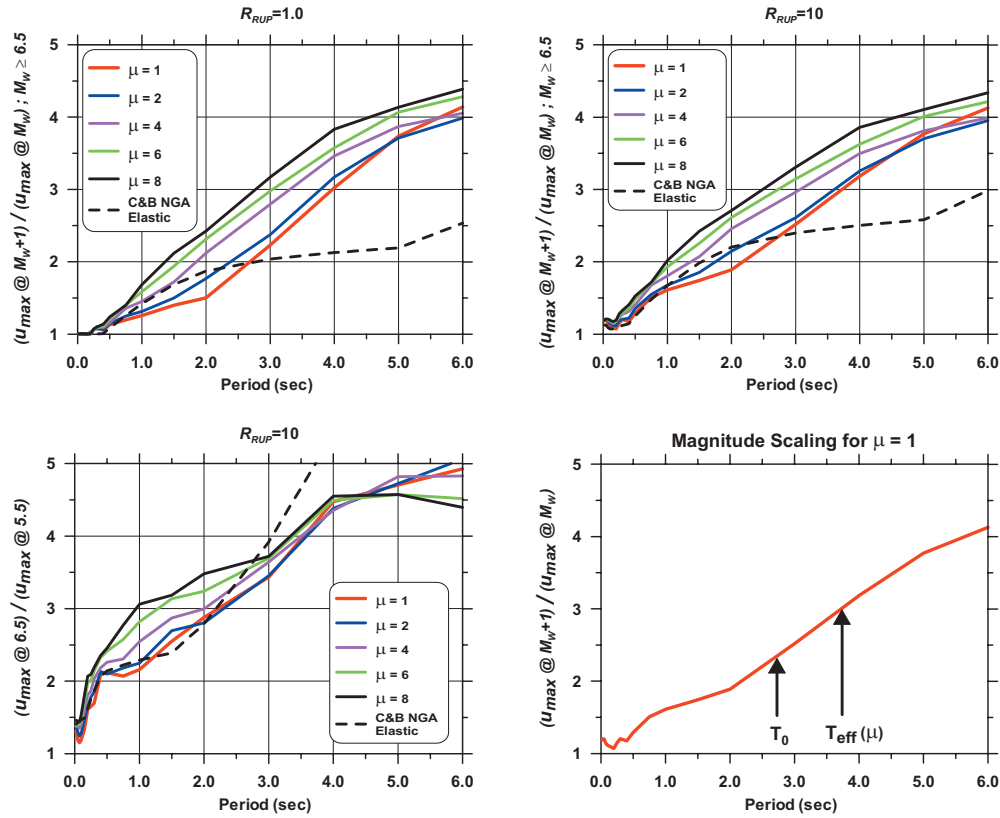


**Figure 11.** Magnitude scaling on median displacement response, i.e., scaling of maximum displacement ( $u_{max}$ ) by increasing one unit magnitude. Bottom right frame conceptually illustrates the effect of period lengthening (due to inelastic deformation) on the magnitude scaling.

tude scaling is a relatively weak function of distance (see Equation 4 in [Bozorgnia et al. 2010](#)).

An interpretation of the above observation that *magnitude scaling is higher at higher ductility levels* is schematically presented in the bottom-right plot of Figure 11. In this plot, two concepts are illustrated: (i) For elastic systems, magnitude scaling generally increases with period, i.e., a larger magnitude earthquake can produce richer long-period ground motions. (ii) Inelastic systems generally exhibit “softening” of effective stiffness, or lengthening of effective period (see e.g., [Iwan and Gates 1979](#); among others). Therefore, an inelastic system with initial period  $T_0$  behaves like an equivalent elastic system with an “effective period”  $T_{eff} \geq T_0$ . Therefore, as the lower-right plot in Figure 11 shows, if elastic response spectra are used, for a system with initial period  $T_0$  the actual magnitude scaling should be associated with a longer period  $T_{eff} \geq T_0$ . Since a larger ductility generally causes a longer  $T_{eff}$ , magnitude scaling becomes larger by increasing ductility. Hence, as stated above, it is generally unconservative to use the magnitude scaling of an elastic system

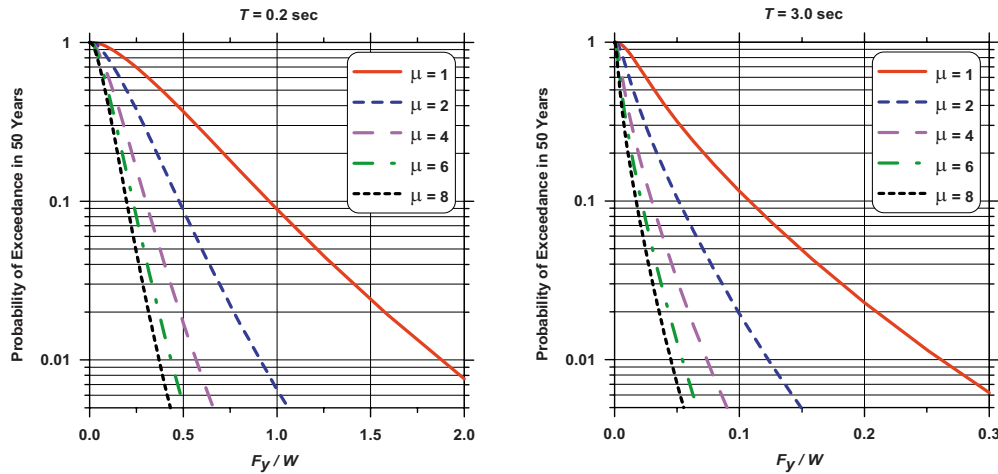


**Figure 12.** Results of probabilistic hazard analyses (PSHA) for  $F_y/W$  at a site in San Francisco, California, for ductility  $\mu=1, 2, 4, 6$  and  $8$ , and for periods  $0.2$  sec (left) and  $3.0$  sec (right), for  $V_{s30}=760$  m/sec,  $Z_{2.5}=1$  km.

to predict inelastic response, especially for  $\mu > 2$ ; and the degree of the unconservatism depends on the ductility level.

### PSHA IMPLEMENTATION OF GMPE FOR INELASTIC SPECTRA

In order to directly perform a probabilistic seismic hazard analysis (PSHA) on inelastic spectra, the developed inelastic GMPE is used as part of a PSHA package. Since our GMPE in this study has the same general form as that developed by [Campbell and Bozorgnia \(2007, 2008\)](#), any PSHA computer package that already incorporates the Campbell and Bozorgnia elastic GMPE, can easily be modified to use our inelastic GMPE. One such PSHA computer package is OpenSHA ([Field et al. 2003](#), [OpenSHA 2009](#)). To demonstrate the concept, we used OpenSHA to carry out inelastic PSHA for a site in San Francisco, California, located about 15 km from the San Andreas Fault. Examples of PSHA results are presented in Figures 12 and 13. Figure 12 shows the probability of exceedance in 50 years for the seismic coefficient  $F_y/W$  for  $T_0=0.2$  and  $3.0$  sec. By choosing the level of probability of exceedance and expected available ductility, one can easily estimate the seismic coefficient  $F_y/W$  demanded by the ground shaking at the site. In such direct PSHA results, there is no need to assume a simplified relationship between elastic and inelastic spectra as is a common practice now.

Figure 13 presents the PSHA example results for maximum inelastic deformations for the same site in San Francisco for periods  $T_0=0.2, 1.0, 3.0$  and  $5.0$  sec. This figure reveals that the maximum deformation of an inelastic system is higher than that for an elastic system, even for long structural periods, especially for low probability of exceedance and large ductility demands. Therefore, for a relatively low probability of exceedance and large

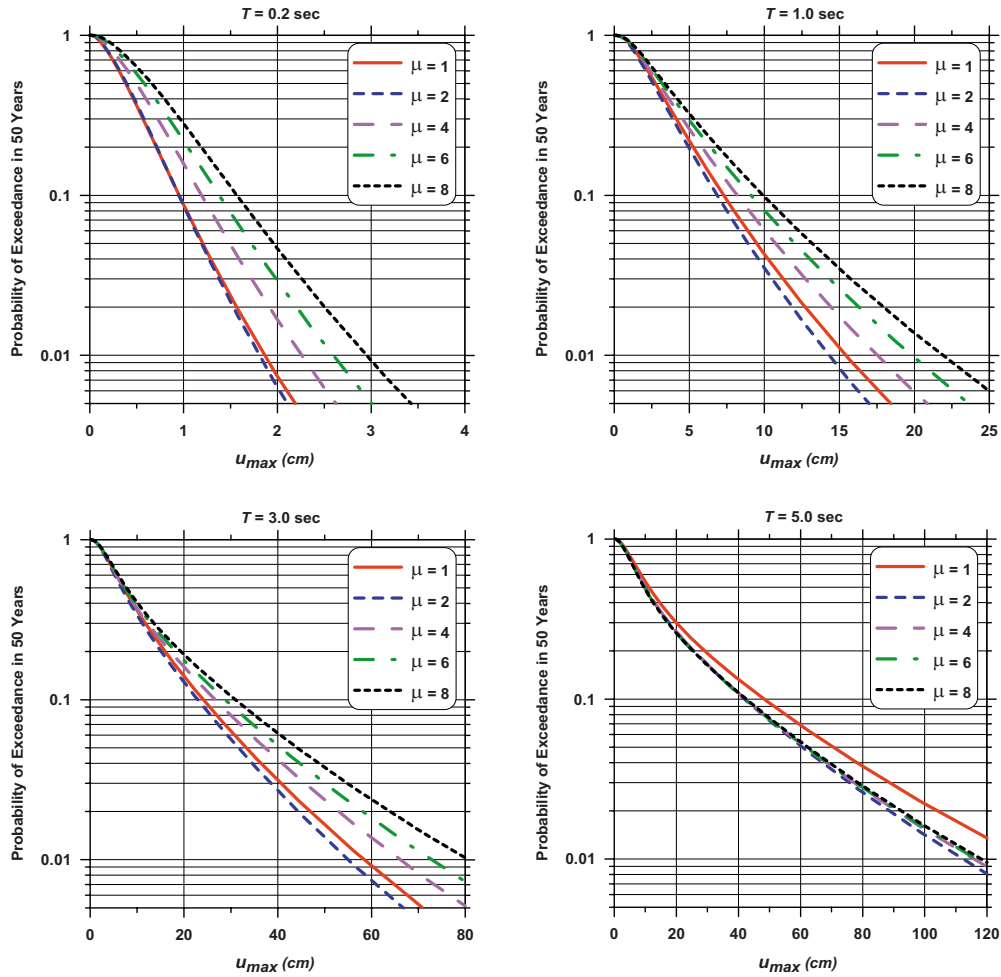


**Figure 13.** Results of PSHA for maximum deformation at a site in San Francisco, California, for ductility  $\mu=1, 2, 4, 6$  and  $8$ , and for periods  $0.2, 1.0, 3.0$ , and  $5.0$  sec, for  $V_{s30} = 760$  m/sec,  $Z_{2.5} = 1$  km.

levels of ductility it is unconservative to carry out a PSHA for an elastic system and assume the constant displacement rule to estimate maximum displacement of an inelastic system.

As Figure 13 shows, for example for  $\mu=6$  and  $T_0=1.0$  sec at 2% probability of exceedance in 50 years (2475 return period), maximum inelastic displacement is about 29% higher than maximum elastic displacement. This same difference is about 22% at  $T_0=3.0$ . It is not until a period of about 5.0 sec that the elastic and inelastic displacements converge. This trend is consistent with the deterministic results presented in the lower right plot of Figure 9. It is also important to note that the PSHA results presented in Figures 12 and 13 are for a site in San Francisco, a place with a potential to experience a large magnitude event. For

other sites farther away from major active faults, or for lower ductility, the PSHA results for inelastic and elastic displacements are closer to each other over a wider period range.

It should be noted that the effects of directivity pulses were not explicitly considered as part of our analysis. Such pulses can have substantial effects on inelastic deformations (see, e.g., [Bertero et al. 1978](#), [Bozorgnia and Mahin 1998](#)).

### SUMMARY AND CONCLUDING REMARKS

We developed and used a large database of inelastic response spectra to formulate a ground motion prediction equation (GMPE, or “attenuation” relationship) for inelastic spectra, as reported in our companion paper ([Bozorgnia et al. 2010](#)). We used this GMPE to directly perform deterministic and probabilistic seismic hazard analyses for inelastic response spectra. The GMPE is associated with different levels of displacement ductility ranging from one (i.e., elastic response) to eight. For each ductility level, the GMPE correlates inelastic spectra to earthquake magnitude, fault mechanism, site-to-source distance, local soil conditions, and basin (sediment) depth. We used our inelastic GMPE in OpenSHA, an open source PSHA computer package, to perform a hazard analysis for inelastic response spectra for a site in San Francisco, California.

The newly developed GMPE for inelastic spectra and its implementation in hazard analyses have revealed that:

- We could verify the pioneering concept of the “equal displacement rule” proposed by A. Veletsos, N. Newmark, and W. Hall; however, its period range of validity is a function of earthquake magnitude and level of ductility. For small and moderate events, and/or for low ductility levels, the constant displacement rule works well over a wide period range. Inelastic displacement will, however, be underestimated if we use the equal displacement rule, even at long periods, for structures that need to sustain a large degree of ductility during a large magnitude earthquake.
- “Magnitude scaling” of inelastic spectra, i.e., increase of inelastic spectral ordinates with increasing earthquake magnitude, is higher than that for elastic spectra, especially for  $\mu > 2$  and magnitudes greater than 6.5. This is mainly due to a combination of two phenomena: (a) larger magnitude events produce richer long-period ground motions; and (b) the effective period of inelastic system increases with increasing ductility level (see Figure 11). It is, therefore, generally unconservative to use magnitude scaling of an elastic system and apply it to an inelastic system, especially for  $\mu > 2$ . The degree of the unconservatism depends on the ductility level.
- Consistent with the deterministic analysis, PSHA results revealed that for a site located near a major active fault system, maximum inelastic displacement is higher than maximum elastic displacement over a wide period range, if the ductility demand is high in a rare seismic event.

Our study shows that a GMPE for inelastic spectral ordinates can easily be implemented as part of a standard PSHA package in order to directly perform probabilistic

seismic hazard analysis for inelastic response, avoiding possible over- or under-conservatism in approximating inelastic deformation from elastic deformation.

### ACKNOWLEDGMENTS

This study was sponsored by the Pacific Earthquake Engineering Research Center's (PEER's) Program of Applied Earthquake Engineering Research of Lifelines Systems supported by the California Department of Transportation and the Pacific Gas and Electric Company. This work made use of the Earthquake Engineering Research Centers Shared Facilities supported by the National Science Foundation, under award number EEC-9701568 through PEER. Any opinions, findings, conclusions, or recommendations expressed in this publication are those of the authors and do not necessarily reflect those of the funding agencies. We thank Ned Field for revising the OpenSHA code to use our GMPE for inelastic spectra. Dr. Campbell was partially sponsored by EQECAT, Inc. Constructive technical discussions with Steve Mahin and Jack Moehle are gratefully appreciated. We thank anonymous reviewers for their comments that much improved the manuscript.

### REFERENCES

- Bertero, V. V., Mahin, S. A., and Herrera, R. A., 1978. Aseismic design implications of near-fault San Fernando earthquake records, *Earthquake Eng. Struct. Dyn.* **6**, 31–42.
- Bozorgnia, Y., and Campbell, K. W., 2004. Engineering characterization of ground motion, in *Earthquake Engineering: From Engineering Seismology to Performance-Based Engineering*, Eds. Bozorgnia and Bertero, CRC Press, Boca Raton, FL.
- Bozorgnia, Y., and Mahin, S. A., 1998. Ductility and strength demands of near-fault ground motions of the Northridge earthquake, *Proceedings, 6th U.S. National Conference on Earthquake Engineering*, Seattle, WA.
- Bozorgnia, Y., Hachem, M. M., and Campbell, K. W., 2010. Ground motion prediction equation (“attenuation relationship”) for inelastic response spectra, *Earthquake Spectra* **26**, 1–23.
- Campbell, K. W., and Bozorgnia, Y., 2007. *Campbell-Bozorgnia NGA ground motion relations for the geometric mean horizontal component of peak and spectral ground motion parameters*, PEER Report No. 2007/02, Pacific Earthquake Engineering Research Center, University of California, Berkeley, 238 pp.
- , 2008. NGA ground motion model for the geometric mean horizontal component of PGA, PGV, PGD and 5% damped linear elastic response spectra for periods ranging from 0.01 to 10 s, *Earthquake Spectra* **24**, 139–171.
- Chopra, A. K., and Chintanapakdee, C., 2004. Inelastic deformation ratios for design and evaluation of structures: single-degree-of-freedom bilinear systems, *ASCE Journal of Structural Engineering* **130**, 1309–1319.
- Federal Emergency Management Agency (FEMA 440), 2005. *Improvement of nonlinear static seismic analysis procedures, ATC-55 Project*, Applied Technology Council, Redwood City, California.
- Field, E. H., Jordan, T. H., and Cornell, C. A., 2003. OpenSHA: A developing community-modeling environment for seismic hazard analysis, *Seismol. Res. Lett.* **74**, 406–419.

- Iwan, W. D., and Gates, N. C., 1979. The effective period and damping of a class of hysteretic structures, *Earthquake Eng. Struct. Dyn.* **7**, 199–211.
- Miranda, E., 2000. Inelastic displacement ratios for structures on firm sites, *ASCE Journal of Structural Engineering* **126**, 1150–1159.
- Newmark, N. M., and Hall, W. J., 1982. *Earthquake Spectra and Design*, Monograph, Earthquake Engineering Research Institute, Oakland, California.
- OpenSHA, 2009. *Open Seismic Hazard Analysis Computer Platform*, <http://www.opensha.org/>
- Riddell, R., 2008. Inelastic response spectrum: Early history, *Earthquake Eng. Struct. Dyn.* **37**, 1175–1183.
- Tothong, P., and Cornell, C. A., 2006. An empirical ground-motion attenuation relation for inelastic spectral displacement, *Bull. Seismol. Soc. Am.* **96**, 2146–2164.
- Veletsos, A. S., and Newmark, N. M., 1960. Effect of inelastic behavior on the response of simple systems to earthquake motions, *Proceedings of the Second World Conference on Earthquake Engineering*, Japan, 2, 895–912.

(Received 17 December 2008; accepted 10 July 2009)